PAPER

A 3D printable diamond polymer composite: a novel material for fabrication of low cost thermally conducting devices†

U. Kalsoom,[a] A. Peristyy,[a] P. N. Nesterenko[ab] and B. Paull*[ab]

The development of a thermally conducting composite material that can be rapidly 3D printed into prototype objects is presented. The composite structures containing 10, 20, 25 and 30% (w/v) of 2–4 micron sized synthetic diamond microparticles added to the acrylate polymer were produced using a low cost stereolithographic 3D printer. The prepared materials were characterised according to heat transfer rates, thermal expansion co-efficients and contact angles, and analysed using high resolution electron microscopy, thermogravimetric analysis and thermal imaging. The composites displayed minor enhancements in heat transfer rates with incrementing diamond content upto 25% (w/v), however a significant improvement was observed for the 30% (w/v) polymer–diamond composite, based on an interconnected diamond aggregate network, as confirmed by high resolution scanning electron microscopy. The developed material was used in the fabrication of prototype 3D printed heat sinks and cooling coils for thermal management applications in electronic and fluidic devices. Infrared thermal imaging performed on 3D printed objects verified the superior performance of the composite compared to the inherent polymer.

Introduction

Polymers are one of the most extensively employed materials because of their unique and widely varying properties, including light weight, strength, ease of manufacturing and ductile nature.[1] However, for the majority of synthetic polymers, poor heat dissipation[2] and high thermal expansion coefficients limits their application in thermally sensitive and/or heat generating devices. Examples include electronics devices, typically equipped with high power density systems to meet the demand for high performance and miniaturisation, resulting in the production of a large amount of heat,[3] where overheating can result in a reduced lifetime or system failure. In such cases, thermal management and material compatibility are critical elements which need to be considered prior to manufacturing.[4,5]

The need for a wider variety of materials demonstrating enhanced thermal properties has led to the development of polymer composite systems,[6–8] that adequately combine the processability and weight/strength properties of the original polymer,[9] with the additional thermal conducting properties of the fillers.[10,11] Ceramic fillers e.g. alumina (Al_2O_3), and silicon carbide (SiC),[10,12] and carbon-based materials, such as graphite[13] and diamonds[14] have all been previously used for the formation of thermally conducting composites, based upon their excellent thermal properties. Among these various fillers, diamond exhibits the highest thermal conductivity [2200 $W\ m^{-1}\ K^{-1}$][15] and mechanical stability, and therefore can be considered as a very promising filler for improving the thermal conductivity of future polymer composites.

There are two types of synthetic diamond powders, namely nanodiamonds and microdiamonds, which can be used as fillers in polymer composites. Detonation nanodiamond powder (DND) is manufactured by detonation synthesis in large quantities and is a comparatively low cost nanocarbon material for a wide range of potential applications, including composites.[16] However, the use of microdiamonds, synthesised at high temperatures and high pressures (HPHT diamond), when used as fillers have proven more successful in increasing the thermal conductivity of the resultant composites.[17,18] In recent years the development of polymer composites using diamond powder (containing DND or micro sized HPHT particles) has been the subject of several studies.[1,16,19–22] For example, Zhang et al. developed epoxy composites using diamond powder, and applied the resultant materials to electronic packaging.[19] A composite containing 68% volume loading of diamond powder was shown to exhibit superior thermal properties (thermal

[a]Australian Centre for Research on Separation Science (ACROSS), School of Physical Sciences Chemistry, University of Tasmania, Private Bag 75, Hobart, Tasmania, 7001, Australia. E-mail: brett.paull@utas.edu.au

[b]ARC Centre of Excellence for Electromaterials Science (ACES), School of Physical Sciences Chemistry, University of Tasmania, Private Bag 75, Hobart, Tasmania, 7001, Australia

conductivity $= 4.1$ W m^{-1} K^{-1}) as compared to the starting epoxy polymer itself (thermal conductivity < 1 W m^{-1} K^{-1}). Similar studies using low density polyethylene and polypropylene diamond powder composites have also been reported.[23,24]

In the majority of the above studies, the polymer–diamond (PD) composites have been produced using a traditional basic casting method. Typically an aqueous suspension of diamond or diamond powder is directly added to the polymer solution[25] and stirred magnetically, followed by sonication for several hours. The polymer diamond suspension is then cast into stainless steel moulds and cured at room temp or *via* heating.[26,27] Clearly, such traditional fabrication methods are time consuming (as the curing of the polymer can sometimes take up to several days)[26] and labour-intensive. Such techniques are certainly not amenable to the introduction of complex internal structures[28] or rapid prototyping.

Over the past decade 3D printing has established itself as a technique of choice for rapid casting/prototyping of polymer objects/devices.[29] 3D printing facilitates the production of complex three dimensional objects with internal structure, and increasing resolution (typically 50–500 μm in modern low cost printers). Using this mould free technology and freely available CAD drawing software, rapid alterations in the preform geometries and dimensions can be made iteratively and on-demand.[30,31] More recently 3D printing is being explored for the production of composite based objects.[32–34] A significant body of work on 3D printing of tricalcium phosphate containing composites has been reported, with a variety of bulk materials, to improve strength, biocompatibility and porosity of the material, for use as bone scaffolds for biomedical applications.[35–38] Additionally there are a limited number of reports in which 3D printing has been employed to produce polymer composite materials exhibiting enhanced optical,[32,34] electrical[33,39] and thermal properties.[40]

Recently, carbon base composites amenable to 3D printing have received considerable attention. For example, conductive carbon black was recently used as a filler for printing a conductive thermoplastic composite using a low-cost 3D printer.[33] In this case the composite material was used for the rapid fabrication of a variety of functional electronic sensors, including piezoresistive sensors capable of sensing mechanical flexing and capacitive sensors printed with the ability to sense the presence and volume of liquids. More recently, a report on 3D printing of a new thermally conducting polymer composite achieved through the introduction of graphene flakes into acrylonitrile–butadiene–styrene (ABS) has been published.[40] In this work, graphene oxide was added to the ABS followed by chemical reduction of the filler to form graphene sheets. The dispersion containing graphene and polymer was precipitated in the presence of deionised water. The developed composite was melted (210 °C) within the 3D printer nozzle, a process known as fused deposition modelling (FDM), for the production of the thermally conducting composites. However, using the FDM process it was not possible to introduce high filler concentrations, as the formation of graphene aggregates was reported at 7.4 wt%, which resulted in blocking of the printer's nozzle.[40]

An exciting alternative approach, which completely avoids the limitations of the FDM based printers for composite production, is stereolithography. In stereolithographic 3D printers, a laser moves along the surface of the liquid polymer (composite phase), curing the polymer layer by layer, until the entire structure is completed.[41] Here there are no nozzles or spray devices likely to experience blockages, and provided the composite suspension is stable and the photopolymerisation process uninhibited, a large variety of composite materials can be readily produced.

In the following paper we report for the first time the 3D printing of a novel, low-cost thermally conductive composite material, based upon commercially available resins for stereolithographic 3D printers and microdiamond particles. The composite material was developed by simply suspending the HPHT diamond microparticles within the commercial acrylate based resin at concentrations as high as 30% (w/v), avoiding any additional chemical reactions or further modifications. The acrylate polymer–diamond suspension was directly introduced into the printer and used for the fabrication of thermally conducting objects to demonstrate potential applications in thermal management in electronic and fluidic devices.

Materials and methods

Chemicals

Miicraft cream resin (BV-001), a commercially available acrylate based polymer, was purchased from Ray Optics Inc. Hsinchu County, Taiwan. Industrial non porous HPHT microdiamond powder (2–4 μm) was obtained from Hunan Real Tech Superabrasive & Tool Co., Ltd. (Changsha, Hunan, China) (particle distribution provided in ESI1†). Sodium hydroxide and nitric acid were obtained from Sigma Aldrich, Sydney, Australia.

Preparation of polymer–diamond composites

Microdiamond powder has been reported to contain impurities such as Si, W, Ta, P, Al, Mn and S which can significantly alter the surface and aggregation properties of diamond microparticles.[42] Therefore, diamond powder was purified prior to use to achieve uncontaminated diamond surfaces using a procedure described elsewhere.[42] This process also removes any silicate coatings which are added to some commercial diamond powders to reduce their tendency to agglomerate. Briefly diamond powder was treated with sodium hydroxide and nitric acid followed by intensive washing with deionised water. The pure microdiamond powder was then kept in an oven at 70 °C until completely dried.

Miicraft cream resin (BV-001) was used for the formation of composites. Acrylate polymer diamond composites (APD-*X*, where "*X*" represents diamond powder concentration) consisting of 10%, 20%, 25% and 30% (w/v) microdiamond concentrations were prepared by adding the appropriate amount of powder to the resin. The APD-*X* mixture was stirred for an hour vigorously with a magnetic stirrer to promote homogeneous dispersion of the particles. This APD-*X* mixture was then sonicated for 30 min to further disperse the diamond microparticles

in the resin. Once prepared the resin consisting of diamond microparticles was used as such without further modifications.

3D printing

A Miicraft 3D (Miicraft, Hsinchu, Taiwan) printer with bottom-up projection was employed for the fabrication of composites. For computer designing of the object, the Inventor Pro software downloaded from the Autodesk website (San Rafael, USA) http://www.autodesk.com was used. The CAD files from the software were converted into the STL files to make them compatible with the Miicraft software. The digital 3D object was sliced into 2D cross sectional layers to produce bitmap images that are read sequentially by the DLP pico-projector (450 ppi) of the printer. The curing time was set at 5 s for 3D printing using the resin. For the APD-X composite, the curing time was set at 15 s for first 5 layers of the print to allow appropriate adhesion of the printing objects and changed to 8 s for rest of the layers throughout the fabrication. The thickness of each layer was set at 50 μm and the printing speed was kept at slow.

For characterisation, rectangular blocks ($l = 23$ mm, $w = 23$ mm, $h = 10$ mm) of AP and APD composite consisting of 10, 20, 25 and 30% (w/v) diamond powder were fabricated.

Heat transfer measurement

For thermal characterisation, the heat transfer across the 3D printed rectangular bars fabricated from the AP and APD-X composite material consisting of various concentrations of diamond microparticles was determined. For heat transfer measurements, a computer controlled heating system as described elsewhere[43] was employed to allow temperature control of the printed blocks in both directions. The APD-X composite under test was placed into the system set at room temperature (20 °C). A thermocouple was placed on the top surface of the block to monitor the temperature. The loss of heat from the block to the surrounding atmosphere was minimised by enclosing the object with insulation foam during the experiment. A schematic representation of the apparatus is provided in ESI (ESI2†).

Scanning electron microscopy

Scanning Electron Microscopy (SEM) imaging was performed on a Hitachi SU70 instrument (Hitachi High Technologies America, USA), and sample preparation involved placing a small cross section of the PD-X materials on to carbon tape on an Al SEM stub. Samples were sputter coated with a thin (approx. 4 nm) layer of platinum prior to imaging at 1.5 kV.

Thermogravimetric analysis

For thermogravimetric analysis, a Labsys Evo instrument, Setaram, Caluire, (France) was employed. Thermogravimetric measurements were performed on AP and APD-30 composite in the presence of air. 10–12 mg of the sample was weighed and placed in aluminium crucible for analysis. The heating rate set at 5 °C min^{-1} was used to raise the temperature from 35–500 °C.

Contact angle measurements

Surface properties of AP and APD composites were characterised by measuring the contact angles of redistilled water droplets placed on the surface of the printed material under study. Photos of the objects were taken and the contact angles were measured using Image J software downloaded from the website (http://rsb.info.nih.gov/ij/download.html). The drops of re-distilled water (with a volume of 6 μL) were placed on a cleaned surface. At least three contact-angle measurements were obtained and averaged.

Linear thermal expansion coefficient

For measurement of coefficient of linear thermal expansion, the rectangular prisms printed from AP and APD-30 composite were placed in the heating system and temperature of the object was raised from 20–45 °C. A thermocouple placed at the top of the block was used to monitor the temperature.

The difference in initial and final length was measured using the Image J software. To make the equipment suitable for Image J software, the scale (mm) was placed on the heating unit. The distance in pixels was converted to millimetres using the scale and change in length (ΔL) was measured. The linear thermal expansion coefficient was measured using the following formula

$$\alpha = \Delta L / (L_o / \Delta T),$$

where, ΔL = change in length of the sample, L_o = original length of the sample, ΔT = temperature change during the test.

IR thermal imaging

In this study the IR camera used for capturing thermal images of the composite heat sink and cooling system was purchased from FLIR (VIC, Australia). FLIR tools software downloaded from (http://flir.custhelp.com/) was used for temperature measurements at various points. AP and APD composite objects were allowed to heat on the heating system set at 100 °C and thermal images were recorded to observe temperature profiles.

Results and discussion

The exact composition of the Miicraft cream resin is proprietary information, but to the best of the authors' knowledge consists of an acrylate monomer (40–60 wt%), an acrylate oligomer (20–35 wt%), a modified acrylate (10–25 wt%), a photoinitiator and additives (5–15 wt%). The specific gravity (ASTM D 1475) and boiling point of the resin are 1.1 g mL^{-1} (25 °C) and >200 °C, respectively.

Initially, the maximum concentration of diamond suspension in the resin whilst remaining suitable for printing was investigated. Above 30% (w/v) microdiamond concentration, poor adhesion of the material with the printer's stage was observed and so limited the diamond content above this concentration.

Printed AP and APD composite rectangular bars ($l = 23$ mm, $w = 23$ mm, $h = 10$ mm) consisting of various concentrations of diamond microparticles ranging from 10–30% were

investigated according to their heat transfer efficiency. Each block was tightly held in direct contact with the heating system set at 20 °C and a thermocouple was placed at the top surface of the block to observe temperature changes. The temperature of the heating system was raised to 100 °C (the system required only few seconds to get to that temperature) and time taken to heat the top surface of 3D printed block from room to target temperatures (up to 60 °C) was recorded. Fig. 1 shows a plot of time *vs.* top surface temperature for APD composite bars consisting of various concentrations of diamond particles. As shown the ability of the composite to transfer heat increases slightly with an increase in microdiamond concentration up to 25% (w/v). However, as the diamond concentration was increased to 30% (w/v), a significant improvement in the heat transfer rate of the composite was noticed, requiring only ~30% of the time for the top surface of the block to reach the target temperature (*i.e.* 60 °C), as compared to the lesser composites. This significant increase in the heat transfer efficiency for the APD-30 composite results from the formation of interconnected diamond microparticle aggregates at concentrations above 30%, as has been demonstrated previously for traditionally cast polymer composite materials.[8]

To understand this behaviour and distribution of diamond microparticles, SEM images of the AP and APD composites were taken. High resolution images of the 3D printed diamond–polymer composite materials with increasing concentrations of diamond particles are shown in Fig. 2. SEM images of the APD-10 composite showed that most of the diamond particles were isolated from each other (Fig. 2b) and this limited contact between microparticles resulting in poor heat transfer capability. However, SEM images of APD-20 and APD-25 (Fig. 2c and d) composites showed a slight improvement in contact between the particles, reflected in small increments in heat transfer efficiency. High resolution images of APD-30 displayed a drastic increase in a number of contact points between the microparticles, showing the formation of highly interconnected diamond aggregates (Fig. 2e and f). This highly connected network of diamond microparticles resulted in the substantial (greater than 200%) improvement in the heat transfer efficiency of the composite.

Fig. 2 SEM images taken from a cross-section of (a) AP (b) APD-10 (c) APD-20 (d) APD-25, and (e)–(f) APD-30 composite materials.

This behaviour of formation of cluster–cluster network has been described previously for carbon based fillers. The conductive particles form aggregates in the composite at relatively low filler contents. As the concentration of filler is increased, the number and size of the clusters increases and above a critical filler concentration, known as percolation threshold, these clusters begin to accumulate in floccules, forming a highly interconnecting network of particles filling the entire volume of the polymer and thus making the material conductive.[44]

This threshold is evident when plotting the relationship between heating time required to raise the composite temperature from 20 to 50 °C *vs.* diamond particle concentrations (Fig. 3). Fig. 3 shows significant drop in heating time above 25% (w/v), thus providing evidence for the presence of a fully interconnected network of diamond particles above this concentration.

Thermogravimetric analysis

In previous reports, thermogravimetric analysis (TGA) has been performed on polymer composites, to observe the impact of introducing the carbon based fillers into the polymeric material.[45,46] Here the effect of diamond microparticles inclusion on the thermal stability of the AP was also studied using TGA. For TGA, samples APD and APD-30 were chosen for comparison. Fig. 4 shows the TGA weight loss results generated on AP and APD composite as a function of temperature. Typical three-step weight-loss curve was observed for both AP and the APD-30 composite in the presence of air. For the acrylate polymer, an
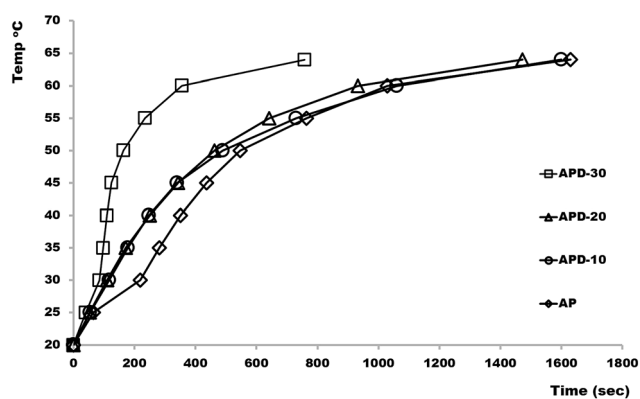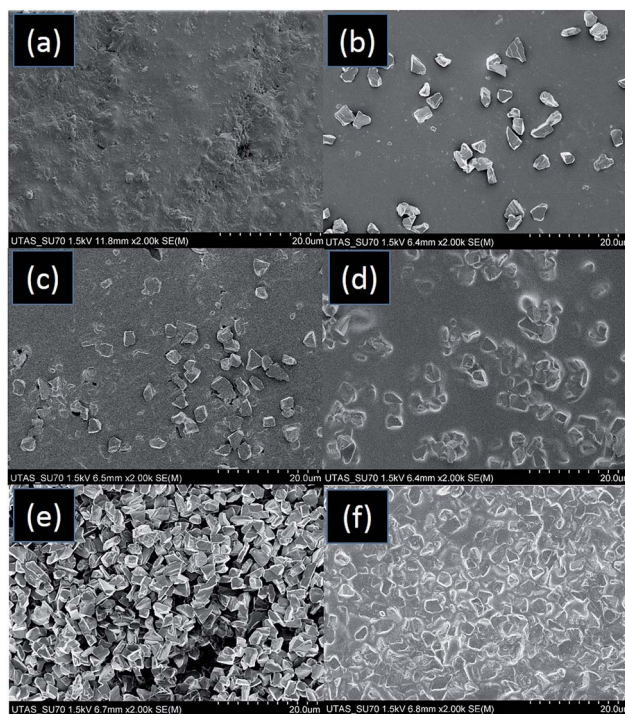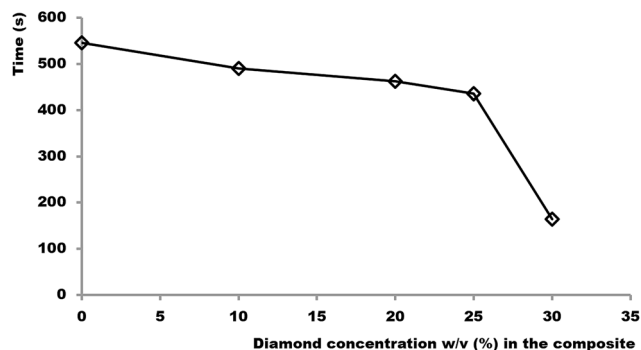

Fig. 1 A plot of time taken with bottom heated 10 mm AP and APD composite blocks for the top surface to rise from 20 °C to target temperatures (25, 30, 35, 40, 45, 50, 55 and 60 °C).

Fig. 3 Plot of heating time required for raising the block temperature from 20 to 50 °C *vs.* concentration of diamond particles in the APD composite.
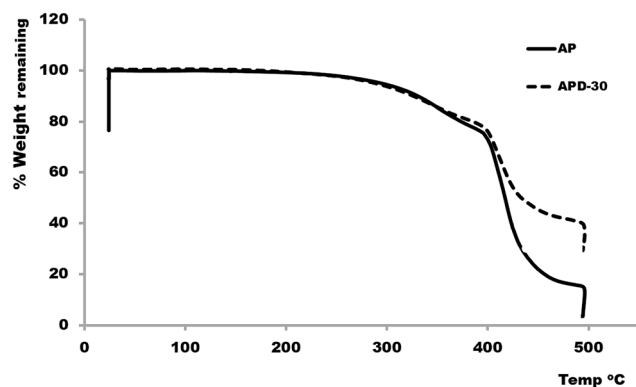

Fig. 4 Thermogravimetric analysis curves for the AP and APD-30 composite.

initial loss in weight (6%) occurred from the dehydration of water molecules from the polymer structures between 100–300 °C. The second weight loss (∼22%) occurred in the range of 300–400 °C due to the decomposition of short chain molecules. However, above 400 °C the weight loss (69%) increased drastically because of the decomposition of the AP at that temperature.

The TGA curve for the APD-30 composite showed significantly different profiles compared to AP. In the first step a small weight loss (6%) occurred once again due to water. In the second step between 300 and 400 °C 19% of the weight was lost, compared to 22% for AP, which is because of the reduced volume of the polymer in the composite. Above 400 °C, the weight of the sample again decreased rapidly, from the degradation of the composite backbone *i.e.* AP leaving only. However, the decomposition of the AP continued slowly until 500 °C, leaving only 46% of the sample weight which included the diamond particles residue itself. The TGA curve for the APD-30 composite demonstrated that in this case the thermal stability of the original polymer in air remains unaffected by the addition of diamond microparticles. These results suggested that diamond microparticles are present in the form of a suspension in the resin which does not significantly affect the chemical structure of the resin and therefore its overall thermal stability.

Contact angle

Changes in thermal properties of materials has previously been observed with increases in hydrophobicity.[47] Hydrophobic surfaces have been known to reduce the interfacial thermal resistance and therefore enhance the thermal conductivity.[48] In previous work on thermally conducting polymer composites, the contact angle of materials has been studied to observe the effect of incorporation of fillers on the surface properties and consequently on thermal behaviour of materials.[16,47] For example, Lu and Ji observed an increase in thermal properties of silicon rubber composites with an increase in hydrophobicity of the surface resulting from incorporation of plasma modified boron nitrite particles.[47] Therefore, the dependence of the surface properties on diamond powder concentration in the APD composite was evaluated by measurement of the (apparent) contact angle of the various 3D printed composites produced herein. The contact angle on the surface of the various composites is listed within Table 1. The presence of diamond particles in the AP matrix resulted in an increase in contact angles, indicating that the wettability of the surface decreases substantially from 0 to 30% diamond. The contact angle of water on the neat AP was measured to be 52.5° ± 2.1 (Fig. 5a), which increases to 98.7° ± 2.4 (Fig. 5b) as the diamond concentration was increased to 30% (w/v).

The results obtained showed how the contact angle kept increasing with an increase in diamond particle concentration in the composite. As the surface of diamond is actually known to be rather hydrophilic rather than hydrophobic, these contact angle measurements are more likely to be a surface roughness effect. It is known that surface roughness will enhance the wettability caused by the chemistry of the surface. In this case the diamond increases the surface roughness (as shown by the SEM images in Fig. 2), but the vast majority of the diamond is beneath a thin surface polymer coating which masks the native

Table 1 Effect of increase in diamond particle concentration on surface wettability

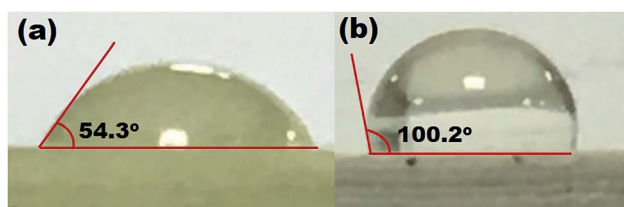| Diamond concentration w/v (%)	Average ($n = 3$) apparent contact angle (θ)
0 (AP)	52.5 ± 2.1
APD-10	85.9 ± 2.2
APD-20	94.6 ± 3.1
APD-30	98.7 ± 2.4

Fig. 5 Contact angle of water on the surface of a (a) AP (b) APD-30 composite.

hydrophilicity of the diamond particles. Thus in this case it's the hydrophobic properties of the acrylate polymer that are enhanced by the increased surface roughness. These results are in agreement with a previous report on diamond polymer composite where an increase in filler concentration resulted in an increase in apparent contact angles.[16]

Linear thermal expansion coefficient

The linear thermal expansion coefficient (LTEC) is a material property that is the measure of the extent to which a material expands on heating.[49] LTEC has been investigated in previous reports to estimate the thermal stability of the newly developed composite materials.[12,14] The introduction of filler with low TEC is expected to lower the thermal expansion of the composite compared to the primary polymeric material, thus improving the thermal stability over time and repetitive heating/cooling cycles.[9]

To evaluate the effect of inclusion of the microdiamond particles on the thermal stability of the 3D printed composite, the LTECs for both the AP and APD-30 composite were determined. The LTEC of diamond itself is 1.18×10^{-6} K^{-1}. Temperature of the AP and APD composite was raised from 20 °C to 45 °C and lengths of the AP and APD-30 composite blocks at both temperatures were measured (Fig. 6). The LTEC value for the polymer was measured to be 180×10^{-6} ($\pm 2.4 \times 10^{-6}$) K^{-1} which falls within the LTEC range previously reported for similar polymers.[50] The inclusion of diamond particles reduced the LTEC value to 48×10^{-6} ($\pm 3.6 \times 10^{-6}$) K^{-1} for APD-30, representing a significant reduction. This observation is in line with many previous studies on composite materials which

have shown that an increase in the concentrations of fillers within polymer matrices can reduce LTECs, as the uniform distribution of the particles within the matrix disrupts the expansion of the polymer chains at high temperature.[50]

Table 2 compares these values with a number of metal and polymer materials. The table highlights how the introduction of the 30% diamond microparticles shifts the LTEC of the composite considerably away from typical polymer values towards values more commonly associated with metal and metal alloys.

Applications of the developed material

Exchange of heat by conduction is usually achieved by introducing a heat sink to dissipate excess heat produced by the

Table 2 Comparison of linear thermal expansion coefficient of common metal, composite and polymer materials[14]

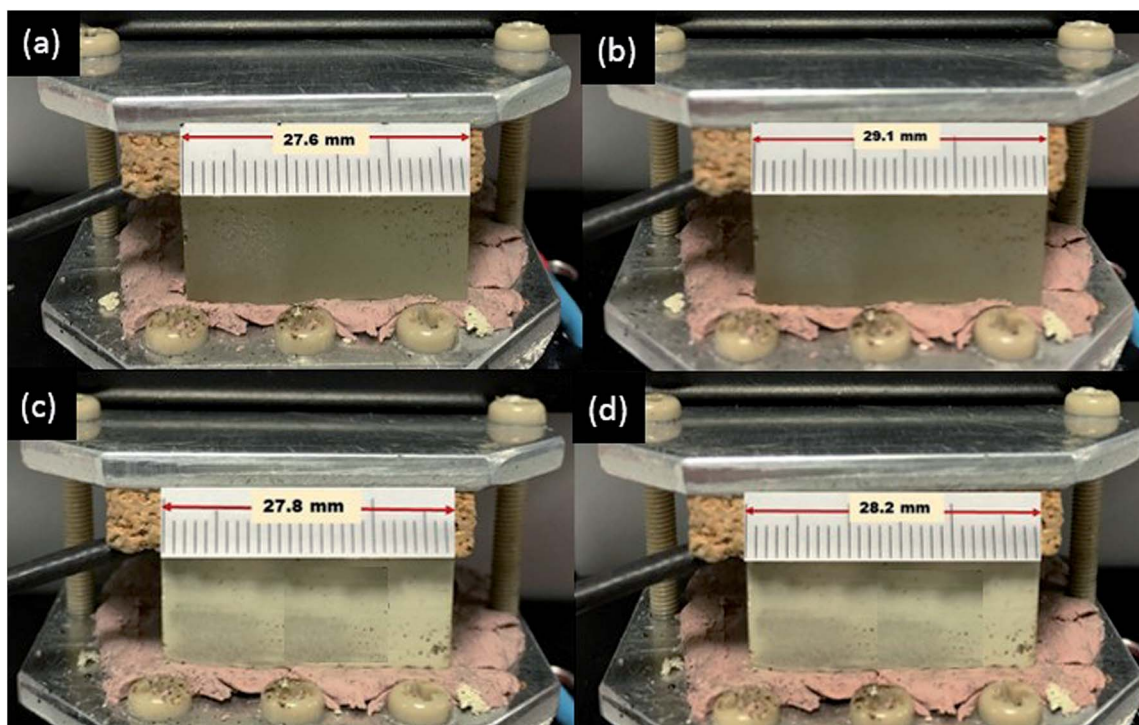| Material	LTEC ($\times 10^{-6}$) K^{-1}
Synthetic diamond	1.1–1.2
Silicon carbide	3.8
Gallium arsenide	5.9
Copper	16.5
Silver	19.8
Aluminium	22
Polytetrafluoroethylene (PTFE)	70–200
High density polyethylene (HDPE)	60–110
Polymethylmethacrylate (acrylic) (PMMA)	50–90
Miicraft cream BV-001 resin (AP)	180
AP–diamond composite (APD-30)	48

Fig. 6 Slides showing (a) initial length of the AP block at 20 °C, (b) final length of the AP block at 45 °C, (c) initial length of the APD-30 block at 20 °C (d) final length of the APD-30 block at 45 °C.

electronic devices.[5] Therefore, to investigate the heat exchanging efficiency of the developed printable material, a heat sink was design and printed using the Miicraft printer using the AP and the APD-30 composite resin. The resultant 3D printed polymer heat sinks are shown in Fig. 7a and b, respectively.

A heating system (as described earlier in the Heat transfer measurement section of the Experimental) was set at 100 °C and used to evaluate the heat transfer performance of the printed sinks. The difference in temperatures and heat distribution of the heat sink printed from the basic AP resin and the APD composite material, each heated for 10 min, was determined using a thermal imaging camera. Thermal images of the two printed heat sinks are given in Fig. 7c and d. Both objects were heated for 10 min and temperatures recorded at three exact positions (*i.e.* top, middle and bottom as shown within the figure). The IR images for the AP and APD-30 composite heat sinks showed that the temperature of the composite heat sink was almost 5–8 °C higher for all three regions (*i.e.* top, middle and bottom) compared to the basic AP heat sink, thus demonstrating clearly how the composite material was indeed providing improved heat distribution away from the heated surface.

Similarly, improved heat transfer properties are also the subject of interest in the design of polymer 'heat pipes', as they are considered as flexible systems for effective thermal control of various heat loaded devices.[51] Therefore, to demonstrate the potential of the printable composite material for application in polymer heat pipes, a 3D coiled cooling system was designed and printed, consisting of a rectangular bar ($l = 30$ mm, $w = 30$ mm, $h = 25$ mm) with a 3 mm hollow internal coil, in both the AP resin and the APD-30 composite material (Fig. 8a and b). Hot water at 40 °C was continuously pumped at constant speed through the coil and once again IR thermal imaging used to capture the heat distribution within the printed blocks. The IR images of the AP cooling system showed that water cooled relatively little as it passed through the coil, with the temperature
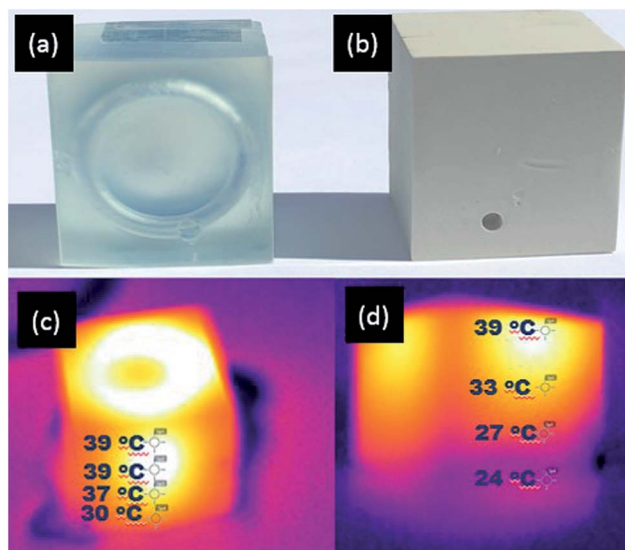

Fig. 8 (a) 3D printed heating coil using commercial resin, (b) 30% (w/v) composite material, (c) IR images of polymer heating coil containing hot water introduced at 40 °C (d) IR image of composite heating coil containing hot water introduced at 40 °C.

of water dropping from 39 °C to 30 °C (Fig. 8c) before it leaves the system. However, the water passing through the APD composite coil was cooled far more efficiently. IR images of the APD-30 composite coil showed a decrease in temperature of the water from 39 °C to 25 °C (room temperature) (Fig. 8d) before exiting the system. These results again demonstrate the superior heat transfer abilities of the APD-30 composite materials compared to the original polymeric material.

Conclusion & future direction

A novel stereolithographic 3D printable thermally conducting material was developed by incorporating up to 30% w/v diamond microparticles in a commercially available acrylate resin. The printed composite material exhibited improved heat transfer rates and significantly decreased thermal expansion coefficients compared to the unmodified starting resin. Demonstration of potential applications of this printable composition were provided in the form of 3D printed heat sinks and heating/cooling coils.

This work has established new possibilities in the rapid fabrication of composite materials using stereolithographic 3D printers. This work can be taken to the next level by developing similar polymer composite with alternative functional fillers *e.g.* magnetic particles and electrically conducting particles for a vast range of applications.
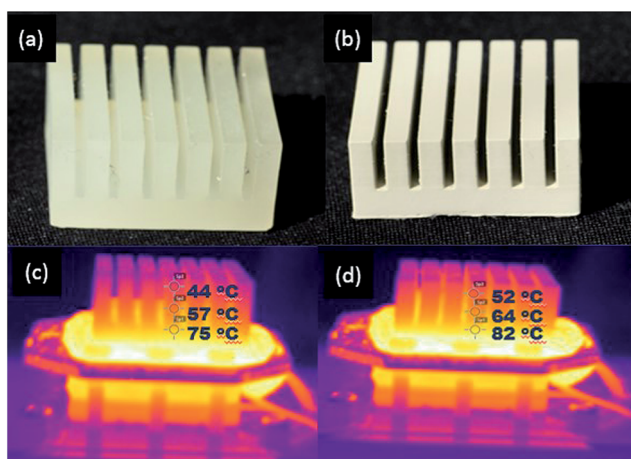
Acknowledgements

Fig. 7 (a) 3D printed heat sink using commercial acrylate resin, (b) 3D printed heat sink using 30% (w/v) composite material, (c) IR images of polymer heat sink heated for 10 min at 100 °C, (d) IR image of composite heat sink heated for 10 min at 100 °C.

References

1 A. Kausar, R. Ashraf and M. Siddiq, *Polym.-Plast. Technol. Eng.*, 2014, **53**, 550–563.

2 K. Gaska, G. Kmita, A. Rybak, R. Sekula, K. Goc and C. Kapusta, *J. Mater. Sci.*, 2015, **50**, 2510–2516.

3 W. Zhou, C. Wang, T. Ai, K. Wu, F. Zhao and H. Guf, *Composites, Part A*, 2009, **40**, 830–836.

4 T. Schubert, B. Trindade, T. Weissgaerber and B. Kieback, *Mater. Sci. Eng., A*, 2008, **475**, 39–44.

5 D. D. L. Chung, *Appl. Therm. Eng.*, 2001, **21**, 1593–1605.

6 H. C. Kuan, C. C. M. Ma, W. P. Chang, S. M. Yuen, H. H. Wu and T. M. Lee, *Compos. Sci. Technol.*, 2005, **65**, 1703–1710.

7 H. Jung-Pyo, Y. Sung-Woon, H. Taeseon, O. Joon-Suk, H. Seung-Chul, L. Youngkwan and N. Jae-Do, *Thermochim. Acta*, 2012, **537**, 70–75.

8 I. A. Tsekmes, R. Kochetov, P. H. F. Morshuis and J. J. Smit, *IEEE Int. Conf. Dielectr. Liq., 16th*, 2013, 678–681.

9 X. Huang, P. Jiang and T. Tanaka, *IEEE Electr. Insul. Mag.*, 2011, **27**, 9–14.

10 G.-W. Lee, M. Park, J. Kim, J. I. Lee and H. G. Yoon, *Composites, Part A*, 2006, **37**, 727–734.

11 T.-L. Li and S. L.-C. Hsu, *J. Phys. Chem.*, 2010, **114**, 6825–6829.

12 C. P. Wong and R. S. Bollamplly, *J. Appl. Polym. Sci.*, 1999, **74**, 3396–3403.

13 W.-L. Song, W. Wang, L. M. Veca, C. Y. Kong, M.-S. Cao, P. Wang, M. J. Meziani, H. Qian, G. E. LeCroy, L. Cao and Y.-P. Sun, *J. Mater. Chem. B*, 2012, **22**, 17133–17139.

14 S. V. Kidalov and F. M. Shakhov, *Materials*, 2009, **2**, 2467–2495.

15 P. N. Nesterenko and P. R. Haddad, *Anal. Bioanal. Chem.*, 2010, **396**, 205–211.

16 F. Şena and M. V. Kahramana, *Polym. Adv. Technol.*, 2014, **25**, 1020–1026.

17 S. V. Kidalov, F. M. Shakhov and A. Ya Vul, *Diamond Relat. Mater.*, 2008, **17**, 844–847.

18 V. N. Mochalin and Y. Gogotsi, *Diamond Relat. Mater.*, 2015, **58**, 161–171.

19 Y. Zhang, X. Hu, J. H. Zhao, K. Sheng, W. R. Cannon, X. Wang and L. Fursin, *IEEE Trans. Compon. Packag. Technol.*, 2009, **32**, 716–723.

20 N. F. Attia, J. P. Rao and K. E. Geckeler, *J. Nanopart. Res.*, 2014, **16**, 1–12.

21 K. D. Behler, A. Stravato, V. Mochalin, G. Korneva, G. Yushin and Y. Gogotsi, *ACS Nano*, 2009, **3**, 363–369.

22 A. Shakun, J. Vuorinen, M. Hoikkanen, M. Poikelispaa and A. Das, *Composites, Part A*, 2014, **64**, 49–69.

23 A.-Y. Jee and M. Lee, *Curr. Appl. Phys.*, 2011, **11**, 1183–1187.

24 A. Zubrowska, R. Masirek, E. Piorkowska and L. Pietrzak, *Polimery*, 2015, **60**, 331–336.

25 J. Y. Lee and D. S. Lim, *Surf. Coat. Technol.*, 2004, **188**, 534–538.

26 S. Morimune, M. Kotera, T. Nishino, K. Goto and K. Hata, *Macromolecules*, 2011, **44**, 4415–4421.

27 O. Shenderova, C. Jones, V. Borjanovic, S. Hens, G. Cunningham, S. Moseenkov, V. Kuznetsov and G. McGuire, *Phys. Status Solidi*, 2008, **205**, 2245–2251.

28 A. Lyons, S. Krishnan, J. Mullins, M. Hodes and D. Hernon, *presented in part at the 20th Annual International Solid Freeform Fabrication Symposium*, Austin, TX, 2009.

29 K. V. Wong and A. Hernandez, *ISRN Mech. Eng.*, 2012, **2012**, 1–10.

30 http://www.approto.com/Media-Center/Additive-vs-Subtractive-Manufacturing–Which-is-Ri.aspx (accessed July 2015).

31 L. S. Dimas, G. H. Bratzel, I. Eylon and M. J. Buehler, *Adv. Funct. Mater.*, 2013, **23**, 4629–4638.

32 E. Tekin, P. J. Smith, S. Hoeppener, A. M. J. van den Berg, A. S. Susha, A. L. Rogach, J. Feldmann and U. S. Schubert, *Adv. Funct. Mater.*, 2007, **17**, 23–28.

33 S. J. Leigh, R. J. Bradley, C. P. Purssell, D. R. Billson and D. A. Hutchins, *PLoS One*, 2012, **7**, e49365.

34 V. Wood, M. J. Panzer, J. Chen, M. S. Bradley, J. E. Halpert, M. G. Bawendi and V. Bulovic, *Adv. Mater.*, 2009, **21**, 1–5.

35 U. Gbureck, E. Vorndran, F. A. Müller and J. E. Barralet, *J. Controlled Release*, 2007, **122**, 173–180.

36 S. T. Becker, H. Bolte, O. Krapf, H. Seitz, T. Douglas, S. Sivananthan, J. Wiltfang, E. Sherry and P. H. Warnke, *Oral Oncol.*, 2009, **45**, e181–e188.

37 Z. Jianhua, Z. Shichang, Z. Min, Z. Yufang, Z. Yadong, L. Zhongtang and Z. Changqing, *J. Mater. Chem. B*, 2014, **2**, 7583–7595.

38 B. G. Compton and J. A. Lewis, *Adv. Mater.*, 2014, **26**, 5930–5935.

39 K. Kordas, T. Mustonen, G. Toth, H. Jantunen, M. Lajunen, C. Soldano, S. Talapatra, S. Kar, R. Vajtai and P. M. Ajayan, *Small*, 2006, **2**, 1021–1025.

40 X. Wei, D. Li, W. Jiang, Z. Gu, X. Wang, Z. Zhang and Z. Sun, *Sci. Rep.*, 2015, **5**, 1–7.

41 B. C. Gross, J. L. Erkal, S. Y. Lockwood, C. Chen and D. M. Spence, *Anal. Chem.*, 2014, **86**, 3240–3253.

42 A. Peristyy, B. Paull and P. N. Nesterenko, *J. Chromatogr. A*, 2015, **1391**, 49–59.

43 S. Sandon, B. Heery, V. Guptaa, D. A. Collins, E. P. Nesterenko, P. N. Nesterenko, M. Talebia, S. Beirnec, F. Thompsonc, G. G. Wallacec, B. Brabazon, F. Regan and B. Paull, *Analyst*, 2014, **139**, 6343–6347.

44 P. Pissis, C. Silvestre, S. Cimmino and D. Duraccio, *Thermoset Nanocomposites for Engineering Applications*, Smithers Rapra Technology Limited, United Kingdom, 2007.

45 C. E. Corcione and M. Frigione, *Materials*, 2012, **5**, 2960–2980.

46 S. Ibrahim and M. R. Johan, *Int. J. Electrochem. Sci.*, 2012, 2596–2615.

47 Y. Lu and T. Ji, *Soc. Plast. Eng*, 2012, 1–3.

48 J. Wang and X.-S. Yi, *Compos. Sci. Technol.*, 2004, **64**, 1623–1628.

49 F. Caverna, *ASM Ready Reference: Thermal properties of metals*, ASM International, USA, 2002.

50 S. Z. D. Cheng, AIS Physics Desk Reference, in *Polymer Physics*, ed. R. E. Cohen, D. R. Lide and G. L. Trigg, Springer, USA, 3rd edn, 2003, pp. 658–690.

51 L. L. Vasiliev, L. P. Grakovich, M. I. Rabetsky and J. L. L. Vasiliev, *Heat Pipe Science and Technology, An International Journal*, 2013, **4**, 251–275.